Dynamic Analysis of Three Snake Robot Gaits

Ryo Ariizumi, *Member, IEEE,* and Fumitoshi Matsuno, *Member, IEEE*

***Abstract*—In the present paper, a dynamic analysis is presented, comparing three snake-like robot gaits: lateral undulation, sidewinding locomotion and sinus-lifting motion. To simplify calculations, sidewinding locomotion and sinus-lifting motion are considered planar movements. Vertical movements are assumed to be small but play a critical role in change where contacts are made. Thus, the normal forces acting on grounded links and the torques applied to pitch joints can be calculated by solving equilibrium equations. The trade-off between locomotion speed and energy efficiency is studied for all three gaits, at eight different environmental settings distinguished by friction coefficients. Simulation results reveal that sinus-lifting motion and sidewinding locomotion are generally more energy efficient gaits than is lateral undulation. More specifically, if the anisotropy in friction is large enough, sinus-lifting motion is the most energy efficient gait; otherwise, sidewinding locomotion is more efficient. However, there are some critical speeds at which the most efficient gait changes, in some environmental settings.**

***Index Terms*—Snake robot, Sidewinding locomotion, Sinus-lifting motion, Energy efficiency**

I. Introduction

SNAKE robots can realize various types of movement, taking advantage of their slim body shape and numerous degrees of freedom. Using this flexibility, they can traverse various environments, negotiate obstacles and even move underwater [1]–[4]. Therefore, they are potentially highly useful for tasks including inspection of pipelines and disaster sites. However, appropriate analysis and control of such a complex system with many degrees of freedom is challenging. Despite this, biological snakes can move over almost any terrain in the real world. Therefore, many researchers are now trying to learn from biological snake gaits to use in snake robots. In turn, we can improve our understanding of biological snakes through studies of robotic ones [5].

Snakes have attracted much attention because of their unique method of locomotion without any legs. However, a reasonable explanation for the serpentine locomotion, called lateral undulation, did not appear until the first quantitative study on snake locomotion was performed by Gray in the 1940's [6]. Based on experiments and measurements of snake gaits, he suggested that forces acting normally to the sides of the body are essential for propulsion by lateral undulation. Gray later suggested that snakes in nature generate their propulsive force by using an anisotropic feature of friction between their surface and the environment [7]. Baio et al. [8] discussed the possibility that they also use lubricant to achieve locomotion. From the viewpoint of robotics, Liljebäck et al. [9] proved that, if viscous friction is assumed, anisotropy in friction is essential for movement of a planar snake robot to be controllable. Hirose [10] modeled a snake as a serial-link mechanism whose links are subject to the velocity constraint that they do not slip sideways. He also proposed the serpenoid curve as the shape of a snake. The serpenoid curve has become the *de facto* standard for the body shape of snake robots [11]–[15]. Justification for use of the serpenoid curve comes not only from biological inspections but also from a control perspective. It has been shown that a body shape similar to the serpenoid curve is generated by solving an optimal control problem [16]. In the literature, the weighted norms of joint angles, angular velocities and angular accelerations are used as the stage cost.

Among the various types of snake locomotion, some are three dimensional, lifting up some parts of body instead of the whole body being in contact with the ground. Sinus-lifting motion is one such gait and is used by many kinds of biological snake. Because this is considered to be more efficient than lateral undulation [10], this gait has also been studied by researchers of snake robots [11]–[14]. These previous studies have mainly investigated the energy efficiency of sinus-lifting motion compared with that of lateral undulation. The motion is approximated as a planar movement and simulations based on simplified dynamic models are discussed. In [14], the authors chose links to be grounded to minimize energy consumption. Their results showed that, through such an optimization, a contact pattern similar to sinus-lifting motion can be generated.

Sidewinding locomotion is also well-known to researchers of snake robots as an efficient type of locomotion. In the first study on sidewinding locomotion by a robot, by Burdick et al. [17], the authors proposed a body shape to realize sidewinding-like locomotion without slipping by a hyper-redundant manipulator. Kelly and Murray [18] described the movement using differential geometry notation, assuming that there is no inertial effect and the net viscous friction is zero. In these works, although sidewinding locomotion is assumed one of the most efficient gaits, they contain no quantitative data on the energy efficiency of the motion. Moreover, the method to determine body shape proposed in [17] leads to discontinuities in curvature, which result in inefficient use of motor torque. In [19], sidewinding locomotion is generated as the result of the maximization of speed through genetic programming. Although this may seem to prove the superiority of sidewinding locomotion over other forms of snake gaits, the authors used an isotropic friction model. Under these conditions, it would be impossible for lateral undulation or sinus-lifting motion to outperform the sidewinding locomotion.

Sidewinding locomotion has been employed in several snake-like robots [20]–[24]. Tesch et al. [25] made snake robots and investigated the energy consumption associated

R. Ariizumi is with the Department of Mechanical Science and Engineering, Graduate School of Engineering, Nagoya University, Nagoya 464-8603, Japan email: ariizumi@nuem.nagoya-u.ac.jp.

F. Matsuno is with the Department of Mechanical Engineering and Science, Graduate School of Engineering, Kyoto University, Kyoto 606-8501, Japan email: matsuno@me.kyoto-u.ac.jp.

with three kinds of locomotion: sidewinding locomotion, rolling, and linear propagation. However, because their robots were not equipped with any mechanism to realize anisotropic friction, it was impossible to realize or investigate lateral undulation and sinus-lifting motion. In [26], the authors studied the dynamics of sidewinding locomotion on slopes in a biological snake compared with that in a snake robot. From observational studies, they suggested a strategy for a snake robot to use sidewinding locomotion to ascend a steep slope. However, little research exists into quantitative comparisons between sidewinding locomotion and either lateral undulation or sinus-lifting motion. This is due to the high calculation cost of simulating sidewinding locomotion, unlike lateral undulation and sinus-lifting motion, which can be accurately simulated using only kinematics and by assuming a no side-slip constraint.

There are many sophisticated approximations for modeling snake robots. For example, in [27], the authors modeled the joints as prismatic, and derived approximate equations of motion. In [28], based on the prismatic joint model, the authors used the averaging method to derive the relationship between the net velocity and the joint angle parameters, where joint angles were parametrized using the serpenoid curve. These approximations work well for control purposes, as they greatly reduce the calculation cost, making them feasible for use in real-time control, and feedback can attenuate any modeling errors. In other studies, to enable more advanced control techniques, differential geometry is also often adopted as in [29], [30]. However, such methods are not necessarily suitable for our purpose.

In the present paper, using various simulations, we compare the energy efficiency of sidewinding locomotion with that of lateral undulation and sinus-lifting motion. As all three gaits are used to move on even surfaces, we are interested in the circumstances in which one gait outperforms the others, in terms of energy efficiency at a certain locomotion speed. The dynamic equations are derived for horizontal movement, assuming anisotropic viscous friction. The movements in the direction of gravity are assumed to be small enough to be considered quasi-static. Using these assumptions, all three gaits can be handled by the same model with a reasonable calculation cost. Simulation results show clear trade-offs between speed and energy efficiency in all three gaits. By plotting energy efficiency against the locomotion speed, the relationship between these trade-offs is illustrated by the boundary of the distribution of points. The points on these boundaries—Pareto fronts, from the optimization point of view—define the best possible energy efficiency as a function of locomotion speed. Intersections of fronts indicate critical speeds at which the most energy efficient gait switches from one to another. The trade-off between speed and power has an inverse trend compared with that of energy efficiency as investigated in the present study. The speed–power relationship was investigated in [31] for lateral undulation, but comparison with other gaits has not been reported, to our knowledge.

Some parts of the present paper appeared in [32]; however, the present paper differs in the following ways: The present paper includes more detailed descriptions of the equations of motion for a planar snake robot, and of the equilibrium

Fig. 1. During sinus-lifting motion [33], a snake lifts only some parts of its body

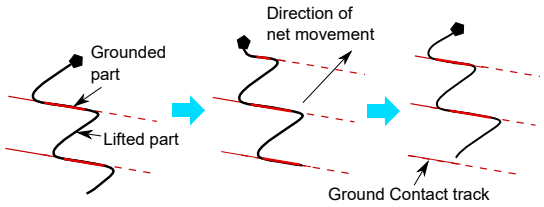

Fig. 2. In sidewinding locomotion, a snake makes contact with ground at two or three points that are at rest. These grounded parts are 'peeled' from the front at the same time following body segments are grounded

equations used to calculate pitch torques and normal forces. We also include sinus-lifting motion in our analysis, since we considered it a very important gait for snake robots. The present paper also includes more accurate and detailed simulation results than the previous version, supporting and adding to our original conclusions.

The remainder of the paper is organized as follows. In Section II, sinus-lifting motion and sidewinding locomotion are explained briefly. A dynamic model of a planar snake robot is described in Section III, along with the equilibrium relations used to determine pitch torque and normal force. Simulation results are shown in Section V, including an explanation of sidewinding locomotion simulation, and a definition of energy efficiency. Finally, Section VI concludes the paper.

II. Sinus-lifting Motion and Sidewinding Locomotion

Sinus-lifting motion, shown in Fig. 1, is a commonly used snake gait for when a snake is moving at high speed [10]. In

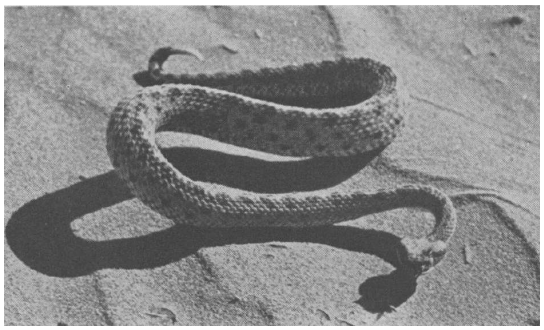

Fig. 3. A sidewinder rattlesnake (*Crotalus cerastes*) moving towards the left of the picture [34]. The snake's body is grounded at two points; most of the body is lifted

this locomotion, the snake lifts up some body parts where the curvature is large, to reduce energy dissipation due to friction without losing the propulsion force attained from body parts with low curvature.

In [10], it is suggested that a snake uses sinus-lifting motion to reduce slippage. Tanaka et al. [11] studied optimal grounding pattern of a wheeled snake robot to reduce constraint force through exhaustive search. The authors showed that this optimization will lead to sinus-lifting-like motion only when the amplitude of body bending is small, which is inconsistent with observations of biological snakes. The results suggested that the minimization of lateral constraint force, which was thought to be important to improve the efficiency of locomotion, may not be the critical factor for sinus-lifting motion. Toyoshima et al. [14] proposed energy efficiency optimizations, and showed that these criteria result in sinus-lifting-like motion with a large bending amplitude, as seen in biological snakes.

Sidewinding locomotion (Fig. 2) is a typical gait for desert snakes, such as the sidewinder rattlesnake, *Crotalus cerastes* (Fig. 3). When sidewinding, a snake's body usually contacts the ground at only two or three segments. The ground-contact segments propagate toward the rear of the snake's body. These segments are at rest relative to the ground and leave a series of parallel straight tracks on the ground. From an observational study of the sidewinder rattlesnake, Mosauer [34] suggested that sidewinding locomotion is particularly suited for movement over sandy terrain at high speed and for long periods. Gray [6] stated that, from the study on sidewinding locomotion of the grass snake, *Tropidonotus natrix*, snakes use sidewinding locomotion on smooth surfaces.

III. Model of the Snake Robot

In this section, we derive a dynamic model of a planar snake robot using the Euler–Lagrange method. We assume that viscous friction acts between the robot and the environment. Further, the friction is assumed to be small in the direction parallel to links and large in the perpendicular direction. This setting is very common in research on snake robots [9], [16], and has been shown to facilitate reasonable simulation of the movement of snake robots. Because of the assumption of anisotropy, lateral undulation and sinus-lifting motion can also be simulated using the same dynamic model, although anisotropy is nonessential for sidewinding locomotion. The Coulomb friction model is also used in some snake robot studies [31]. Although the quantitative properties of gait performance change if Coulomb friction is considered, we have empirically confirmed that the qualitative properties do not change. Moreover, inclusion of Coulomb friction clutters the discussion with two additional variables. Therefore, we do not include Coulomb friction in the present paper.

Another method of deriving the dynamic model based on Newton–Euler method can be found in [15], [31]; however, we consider the Newton–Euler method to be more prone to errors, since it is less methodical and requires a deep understanding of forces acting on each link and joint. In [35], the authors propose the Gibbs–Appell method to derive the equations of motion for a snake robot with lateral constraints. Although the Gibbs–Appell method is well suited to model robots with non-holonomic constraints, there are few advantages when modeling snake robots. After deriving the equations of motion for planar movement, the equilibrium equations required to calculate normal forces and pitch torques are described. Then, using the joint toques gained by solving those equations, energy consumption at each joint is explained.

A. Notation

We consider a snake robot with n links of equal length connected by $n-1$ 2-DOF active joints (in the order of yaw and pitch from the front), as shown in Fig. 4. To keep the model uncluttered, we assume that movements in the direction of gravity are small enough for the inertial effect in this direction to be neglected. We leave the consideration of upright movement to our future research. However, given that the lift-up of some biological snakes such as the grass snake is also not so large, as suggested in [6], this simplification is not so unrealistic. The lifted links of the snake robot are regarded as having no friction force from the ground; grounded links are regarded as the links on which a friction force acts (Fig. 5).

Notation used in the present paper is defined as follows:

l : Half of the length of each link
θ_i : Orientation of link i
ϕ_i : Yaw angle of joint i. $\phi_i = \theta_{i+1} - \theta_i$
(x_h, y_h) : Position of the head
$\boldsymbol{w}$: $\boldsymbol{w} = [x_h \;\; y_h \;\; \theta_1]^T$
$\boldsymbol{x}_i$: Position vector of the center of link i, expressed as $\boldsymbol{x}_i = [x_i \;\; y_i]^T$
$\boldsymbol{x}$, $\boldsymbol{y}$: $\boldsymbol{x} = [x_1 \;\cdots\; x_n]^T$, $\boldsymbol{y} = [y_1 \;\cdots\; y_n]^T$
$\boldsymbol{\theta}, \boldsymbol{\phi}$: $\boldsymbol{\theta} = [\theta_1 \;\cdots\; \theta_n]^T$, $\boldsymbol{\phi} = [\phi_1 \;\cdots\; \phi_{n-1}]^T$
$\bar{\boldsymbol{q}}$: General coordinate. $\bar{\boldsymbol{q}} = [x_h \;\; y_h \;\; \boldsymbol{\theta}^T]^T$

The local coordinate of link i is fixed on the center of mass (CM) of link i, with x^i axis and y^i axis, which incline by θ_i from global x and y respectively.

Vector valued trigonometric functions with vector valued inputs are defined as follows:

$$\begin{aligned} \cos\boldsymbol{\theta} &= \begin{bmatrix}\cos\theta_1 & \cos\theta_2 & \cdots & \cos\theta_n\end{bmatrix}^T, \\ \sin\boldsymbol{\theta} &= \begin{bmatrix}\sin\theta_1 & \sin\theta_2 & \cdots & \sin\theta_n\end{bmatrix}^T. \end{aligned} \tag{1}$$

Diagonal matrices whose diagonal components are trigonometric functions are defined as follows:

$$\begin{aligned} C_\theta &= \mathrm{diag}(\cos\theta_1, \;\cos\theta_2, \;\cdots, \;\cos\theta_n), \\ S_\theta &= \mathrm{diag}(\sin\theta_1, \;\sin\theta_2, \;\cdots, \;\sin\theta_n). \end{aligned} \tag{2}$$

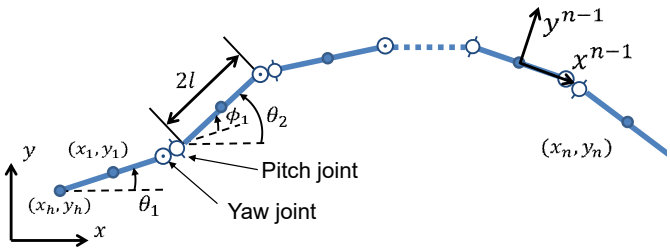

Fig. 4. Schematic of a snake robot (top view) with n links and $n-1$ 2-DOF joints. The head position is (x_h, y_h), the center of mass (CM) of link i is located at (x_i, y_i), the orientation of link i is θ_i, and the angle of yaw of joint i is ϕ_i.

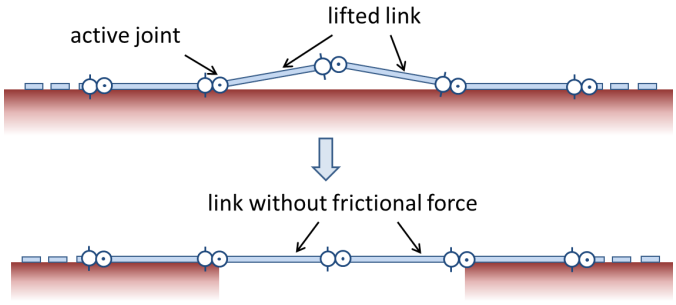

Fig. 5. Handling of the lifting effect. We model lifted links as links that are not subject to any force from the ground

B. Dynamic Model of Planar Snake Robot

The CM of the links is calculated as

$$\begin{cases} x_1 &= x_h + l\cos\theta_1 \\ x_2 &= x_h + 2l\cos\theta_1 + l\cos\theta_2 \\ &\vdots \\ x_n &= x_h + \sum_{i=1}^{n-1} 2l\cos\theta_i + l\cos\theta_n \end{cases}, \tag{3}$$

$$\begin{cases} y_1 &= y_h + l\sin\theta_1 \\ y_2 &= y_h + 2l\sin\theta_1 + l\sin\theta_2 \\ &\vdots \\ y_n &= y_h + \sum_{i=1}^{n-1} 2l\sin\theta_i + l\sin\theta_n \end{cases}. \tag{4}$$

This can be summarized into the following vector notation:

$$\begin{cases} \boldsymbol{x} &= \boldsymbol{e}x_h + lK\cos\boldsymbol{\theta} \\ \boldsymbol{y} &= \boldsymbol{e}y_h + lK\sin\boldsymbol{\theta} \end{cases}, \tag{5}$$

where K and the vector $\boldsymbol{e}$ are defined as follows:

$$K = \begin{bmatrix} 1 & 0 & \cdots & & 0 \\ 2 & 1 & \cdots & & 0 \\ \vdots & \vdots & \ddots & & \vdots \\ 2 & 2 & \cdots & 2 & 1 \end{bmatrix} \in \mathbb{R}^{n\times n}, \tag{6}$$

$$\boldsymbol{e} = [1\ 1\ \cdots\ 1]^T \in \mathbb{R}^n. \tag{7}$$

By differentiating both sides of (5) with respect to time, the velocity relationship can be obtained as

$$\begin{aligned} \dot{\boldsymbol{x}} &= \boldsymbol{e}\dot{x}_h - lKS_\theta\dot{\boldsymbol{\theta}} = \begin{bmatrix} \boldsymbol{e} & \boldsymbol{0} & -lKS_\theta \end{bmatrix}\dot{\bar{\boldsymbol{q}}} = J_{\bar{q}x}\dot{\bar{\boldsymbol{q}}}, \\ \dot{\boldsymbol{y}} &= \boldsymbol{e}\dot{y}_h + lKC_\theta\dot{\boldsymbol{\theta}} = \begin{bmatrix} \boldsymbol{0} & \boldsymbol{e} & lKC_\theta \end{bmatrix}\dot{\bar{\boldsymbol{q}}} = J_{\bar{q}y}\dot{\bar{\boldsymbol{q}}}, \\ \dot{\boldsymbol{\theta}} &= \begin{bmatrix} O_{n\times 2} & I_n \end{bmatrix}\dot{\bar{\boldsymbol{q}}}, \end{aligned} \tag{8}$$

where I_k is a $k\times k$ identity matrix and

$$\begin{aligned} J_{\bar{q}x} &= \begin{bmatrix} \boldsymbol{e} & \boldsymbol{0} & -lKS_\theta \end{bmatrix}, \\ J_{\bar{q}y} &= \begin{bmatrix} \boldsymbol{0} & \boldsymbol{e} & lKC_\theta \end{bmatrix}. \end{aligned} \tag{9}$$

Because motion in the vertical direction is assumed to be so small that it can be neglected, the Lagrangian of the robot comprises only its kinetic energy T

$$T = \frac{1}{2}(\dot{\boldsymbol{x}}^T M\dot{\boldsymbol{x}} + \dot{\boldsymbol{y}}^T M\dot{\boldsymbol{y}} + \dot{\boldsymbol{\theta}}^T J\dot{\boldsymbol{\theta}}) = \frac{1}{2}\dot{\bar{\boldsymbol{q}}}^T\bar{H}\dot{\bar{\boldsymbol{q}}}, \tag{10}$$

where M and J are the matrices with mass and moments of inertia, respectively, of links on their diagonal components. Inertia matrix $\bar{H}$ is defined as follows:

$$\begin{aligned} \bar{H} &:= J_{\bar{q}x}^T M J_{\bar{q}x} + J_{\bar{q}y}^T M J_{\bar{q}y} + \bar{J}, \\ \bar{J} &= \begin{bmatrix} O_2 & O_{2\times n} \\ O_{n\times 2} & J \end{bmatrix}, \end{aligned} \tag{11}$$

which is a symmetric positive-definite matrix.

Viscous friction is assumed to act only on the CM of a link given that the integration of the friction force in the case of pure rotation leads to the formula given in [31]. The viscous coefficients between the environment and the link i are $c_{x,i}$ in the x^i direction, $c_{y,i}$ in the y^i direction and $c_{\theta,i}$ in the rotational direction. Let the rotation matrix which relates the local frame of link i and the global frame be ${}^G R_i$, then the dissipation function for link i is

$$\mathcal{R}_i = \frac{1}{2}\dot{\boldsymbol{x}}_i^T\,{}^G R_i \begin{bmatrix} c_{x,i} & 0 \\ 0 & c_{y,i} \end{bmatrix} ({}^G R_i)^T\dot{\boldsymbol{x}}_i + \frac{1}{2}c_{\theta,i}\dot{\theta}_i^2. \tag{12}$$

By adding them for all of the links, the dissipation function for the entire robot can be derived as

$$\mathcal{R} = \frac{1}{2}\dot{\bar{\boldsymbol{q}}}^T(C_{\mathrm{tr}} + C_{\mathrm{rot}})\dot{\bar{\boldsymbol{q}}} = \frac{1}{2}\dot{\bar{\boldsymbol{q}}}^T\bar{C}\dot{\bar{\boldsymbol{q}}}, \tag{13}$$

where

$$C_{\mathrm{tr}} = J_{\bar{q}xy}^T \begin{bmatrix} C_xC_\theta^2 + C_yS_\theta^2 & (C_x - C_y)S_\theta C_\theta \\ (C_x - C_y)S_\theta C_\theta & C_xS_\theta^2 + C_yC_\theta^2 \end{bmatrix} J_{\bar{q}xy}, \tag{14}$$

$$C_{\mathrm{rot}} = \mathrm{diag}(0,\ 0,\ c_{\theta,1},\ \cdots,\ c_{\theta,n}), \tag{15}$$

$$J_{\bar{q}xy} = \begin{bmatrix} J_{\bar{q}x}^T & J_{\bar{q}y}^T \end{bmatrix}^T, \tag{16}$$

$$C_x = \mathrm{diag}(c_{x,1},\ \cdots,\ c_{x,n}), \tag{17}$$

$$C_y = \mathrm{diag}(c_{y,1},\ \cdots,\ c_{y,n}). \tag{18}$$

Then, Lagrange's equations of motion are written as

$$\frac{d}{dt}\left(\frac{\partial T}{\partial\dot{\bar{\boldsymbol{q}}}}\right)^T - \left(\frac{\partial T}{\partial\bar{\boldsymbol{q}}}\right)^T + \left(\frac{\partial\mathcal{R}}{\partial\dot{\bar{\boldsymbol{q}}}}\right)^T = \bar{E}\boldsymbol{\tau}, \tag{19}$$

where $\bar{E}\in\mathbb{R}^{n\times(n-1)}$ is a coefficient matrix and $\boldsymbol{\tau}\in\mathbb{R}^{n-1}$ is torque applied to the yaw joints. The first term of the left-hand side is

$$\begin{aligned} \frac{d}{dt}\left(\frac{\partial T}{\partial\dot{\bar{q}}}\right) &= \ddot{\bar{q}}^T\bar{H} + \dot{\bar{q}}^T\dot{\bar{H}} \\ &= \ddot{\bar{q}}^T\bar{H} + \dot{\bar{q}}^T\Big(\dot{J}_{\bar{q}x}^T M J_{\bar{q}x} + J_{\bar{q}x}^T M\dot{J}_{\bar{q}x} \\ &\quad + \dot{J}_{\bar{q}y}^T M J_{\bar{q}y} + J_{\bar{q}y}^T M\dot{J}_{\bar{q}y}\Big), \end{aligned} \tag{20}$$

which leads to the following result:

$$\frac{d}{dt}\left(\frac{\partial T}{\partial \dot{\bar{q}}}\right) = \ddot{\bar{q}}^T \bar{H} + \dot{\bar{q}}^T \Big\{ \dot{\bar{Q}} \left(\mathcal{J}_x^T M J_{\bar{q}x} + \mathcal{J}_y^T M J_{\bar{q}y} \right) + \left(J_{\bar{q}x}^T M \mathcal{J}_x + J_{\bar{q}y}^T M \mathcal{J}_y \right) \dot{\bar{Q}} \Big\}, \quad (21)$$

where $\bar{Q} = \mathrm{diag}(\bar{q}_1, \cdots, \bar{q}_{n+2}) = \mathrm{diag}(x_h, y_h, \theta_1, \cdots, \theta_n)$ and

$$\begin{aligned} \mathcal{J}_x &:= \begin{bmatrix} O_{n\times 2} & -lKC_\theta \end{bmatrix}, \\ \mathcal{J}_y &:= \begin{bmatrix} O_{n\times 2} & -lKS_\theta \end{bmatrix}. \end{aligned} \quad (22)$$

The ith component of the second term of the left-hand side of (19) is

$$\begin{aligned} \frac{\partial T}{\partial \bar{q}_i} &= \frac{1}{2}\dot{\bar{\boldsymbol{q}}}^T \frac{\partial \bar{H}}{\partial \bar{q}_i}\dot{\bar{\boldsymbol{q}}} \\ &= \frac{1}{2}\dot{\bar{\boldsymbol{q}}}^T \left(\frac{\partial J_{\bar{q}x}^T}{\partial \bar{q}_i} M J_{\bar{q}x} + J_{\bar{q}x}^T M \frac{\partial J_{\bar{q}x}}{\partial \bar{q}_i} \right. \\ &\quad \left. + \frac{\partial J_{\bar{q}y}^T}{\partial \bar{q}_i} M J_{\bar{q}y} + J_{\bar{q}y}^T M \frac{\partial J_{\bar{q}y}}{\partial \bar{q}_i} \right) \dot{\bar{\boldsymbol{q}}} \\ &= \dot{\bar{\boldsymbol{q}}}^T \left(J_{\bar{q}x}^T M \frac{\partial J_{\bar{q}x}}{\partial \bar{q}_i} + J_{\bar{q}y}^T M \frac{\partial J_{\bar{q}y}}{\partial \bar{q}_i} \right) \dot{\bar{\boldsymbol{q}}}. \end{aligned} \quad (23)$$

Because $J_{\bar{q}x}$ and $J_{\bar{q}y}$ do not depend on $\bar{q}_1 = x_h$ and $\bar{q}_2 = y_h$, it can be seen that

$$\frac{\partial J_{\bar{q}x}}{\partial \bar{q}_i} = \frac{\partial J_{\bar{q}y}}{\partial \bar{q}_i} = O_{n\times(n+2)}, \quad i = 1,\ 2. \quad (24)$$

For $j = 1, \cdots, n$, it holds that

$$\begin{aligned} &\frac{\partial J_{\bar{q}x}}{\partial \bar{q}_{j+2}} \\ &\quad = \begin{bmatrix} O_{n\times 2} & -lK\mathrm{diag}(0,\ \cdots,\ 0,\ \cos\theta_j,\ 0,\ \cdots,\ 0) \end{bmatrix}, \\ &\frac{\partial J_{\bar{q}y}}{\partial \bar{q}_{j+2}} \\ &\quad = \begin{bmatrix} O_{n\times 2} & -lK\mathrm{diag}(0,\ \cdots,\ 0,\ \sin\theta_j,\ 0,\ \cdots,\ 0) \end{bmatrix}. \end{aligned} \quad (25)$$

Therefore, we have

$$\frac{\partial J_{\bar{q}x}}{\partial \bar{\boldsymbol{q}}_i}\dot{\bar{\boldsymbol{q}}} = \mathcal{J}_x \begin{bmatrix} 0 & \cdots & 0 & \dot{\bar{q}}_{i-2} & 0 \cdots & 0 \end{bmatrix}^T, \quad (26)$$

$$\frac{\partial J_{\bar{q}y}}{\partial \bar{\boldsymbol{q}}_i}\dot{\bar{\boldsymbol{q}}} = \mathcal{J}_y \begin{bmatrix} 0 & \cdots & 0 & \dot{\bar{q}}_{i-2} & 0 \cdots & 0 \end{bmatrix}^T, \quad (27)$$

and consequently,

$$\frac{\partial T}{\partial \dot{\bar{\boldsymbol{q}}}} = \dot{\bar{\boldsymbol{q}}}^T \left(J_{\bar{q}x}^T M \mathcal{J}_x + J_{\bar{q}y}^T M \mathcal{J}_y \right) \dot{\bar{Q}}. \quad (28)$$

Regarding the third term of (19), by noting that $\bar{C}$ is symmetric, we get

$$\frac{\partial \mathcal{R}}{\partial \dot{\bar{\boldsymbol{q}}}} = \dot{\bar{\boldsymbol{q}}}^T \bar{C}. \quad (29)$$

Summarizing the above equations, we obtain the following equations of motion:

$$\begin{aligned} \bar{H}\ddot{\bar{\boldsymbol{q}}} + \bar{W}\mathrm{diag}(\dot{\bar{\boldsymbol{q}}})\dot{\bar{\boldsymbol{q}}} + \bar{C}\dot{\bar{\boldsymbol{q}}} &= \bar{E}\boldsymbol{\tau}, \\ \bar{W} &= J_{\bar{q}x}^T M \mathcal{J}_x + J_{\bar{q}y}^T M \mathcal{J}_y, \end{aligned} \quad (30)$$

where $\bar{W}\mathrm{diag}(\dot{\bar{\boldsymbol{q}}})\dot{\bar{\boldsymbol{q}}}$ is the term for Coriolis and centrifugal forces.

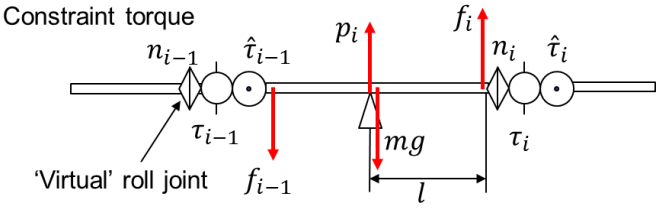

Fig. 6. Illustration of force in vertical direction and torque (side view). Virtual roll joints are added to consider the constraint torque in the roll direction.

The normal force acting on link i and the constraint force at joint i in the vertical direction are p_i and f_i respectively. Torques applied to i-th roll, pitch, and yaw joints are n_i, $\hat{\tau}_i$, and τ_i respectively.

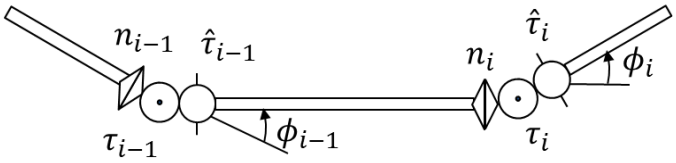

Fig. 7. Illustration of torque (top view). By noticing that the torque can be expressed as a vector in the direction of the rotation axis, the effect of bending at yaw joints can be correctly incorporated into the equilibrium equations

Thus far, we have used generalized coordinates which are suitable for derivation of equations of motion. However, for designing control inputs for yaw joints, it is more convenient to use another coordinate system defined as $\boldsymbol{q} = [x_h \ \ y_h \ \ \theta_1 \ \ \boldsymbol{\phi}^T]^T$. There is a relationship between two types of generalized coordinate system, as follows:

$$\begin{aligned} \dot{\bar{\boldsymbol{q}}} &= J_{q\bar{q}}\dot{\boldsymbol{q}}, \\ J_{q\bar{q}} &= \mathrm{block\,diag}(I_2, J_{\phi\theta}), \\ J_{\phi\theta} &= \begin{bmatrix} 1 & 0 & \cdots & 0 \\ 1 & 1 & \cdots & 0 \\ \vdots & \vdots & \ddots & \vdots \\ 1 & 1 & \cdots & 1 \end{bmatrix} \in \mathbb{R}^{n\times n}. \end{aligned} \quad (31)$$

Substituting (31) into (30), and multiplying both sides of (30) by $J_{q\bar{q}}^T$, we get

$$H\ddot{\boldsymbol{q}} + W\mathrm{diag}(J_{q\bar{q}}\dot{\boldsymbol{q}})J_{q\bar{q}}\dot{\boldsymbol{q}} + C\dot{\boldsymbol{q}} = E\boldsymbol{\tau}, \quad (32)$$

where $H = J_{q\bar{q}}^T \bar{H} J_{q\bar{q}}$, $W = J_{q\bar{q}}^T \bar{W}$, $C = J_{q\bar{q}}^T \bar{C} J_{q\bar{q}}$ and $E = J_{q\bar{q}}^T \bar{E} = [O_{(n-1)\times 3}^T \ \ I_{n-1}]^T$. Note that after multiplication by $J_{q\bar{q}}^T$, the inertia matrix H becomes a symmetric positive-definite matrix.

C. Equilibrium Equations in the Vertical Direction

In the previous subsection, only the planar motion is considered, and used to obtain torques applied to yaw joints. However, we also need the torques applied to the pitch joints, to evaluate energy consumption. In [14], assuming that the snake robot can be approximated as an elastic straight beam, they applied Clapeyron's three-moment equation to determine the pitch torques and normal forces. However, in doing so, the shape of the snake robot and the constraint that the normal force should be in the upward direction are neglected. Therefore, this simplification can be a major deviation from

the energy consumption of real snake robots. In the present study, to obtain these values, the equilibrium equations in the vertical direction are considered; thus, both the shape of the snake robot and the unidirectional constraint can be taken into account.

Let p_i be the normal force acting on link i where $p_i = 0$ if link i is a lifting link, $\hat{\tau}_i$ be the torque applied to pitch joint i, and f_i be the constraint force acting on joint i which prevents links i and $i+1$ from separating in the vertical direction. Let n_i be the constraint torque in the roll direction at joint i, which can be seen as the torque applied to the virtual roll joint located in front of the yaw joint. Note that we assume that the normal force acts on the CG of the link and joints have zero length. Let m be the mass of a link and g be the gravitational acceleration. This notation is illustrated in Figs. 6 and 7. The equilibrium equations for link i can be written as

$$\begin{aligned} &f_i - f_{i-1} + p_i = mg, \\ &\sin\phi_{i-1}\cdot n_{i-1} + \cos\phi_i \cdot \hat{\tau}_i - \hat{\tau}_{i-1} - l(f_i + f_{i-1}) = 0, \\ &n_i - \cos\phi_{i-1}\cdot n_{i-1} - \sin\phi_i \cdot \hat{\tau}_i = 0. \end{aligned} \tag{33}$$

Deriving these equations on every link, the following linear equations can be derived:

$$D\boldsymbol{f} = mg\boldsymbol{e} - \boldsymbol{p} = mg\boldsymbol{e} - S\boldsymbol{r}, \tag{34}$$

$$\tilde{S}_\phi \boldsymbol{n} + D_c\hat{\boldsymbol{\tau}} - lA\boldsymbol{f} = \boldsymbol{0}, \tag{35}$$

$$\bar{D}_c\boldsymbol{n} - \bar{S}_\phi\hat{\boldsymbol{\tau}} = \boldsymbol{0}, \tag{36}$$

where the matrix D_c and $\bar{D}_c$ are defined as

$$D_c = \begin{bmatrix} \cos\phi_1 & 0 & \cdots & 0 & 0 \\ -1 & \cos\phi_2 & \cdots & 0 & 0 \\ \vdots & \vdots & \ddots & \vdots & \vdots \\ 0 & 0 & \cdots & -1 & \cos\phi_{n-1} \\ 0 & 0 & \cdots & 0 & -1 \end{bmatrix} \in \mathbb{R}^{n\times(n-1)}, \tag{37}$$

$$\bar{D}_c = -\begin{bmatrix} -1 & 0 & \cdots & 0 & 0 \\ \cos\phi_1 & -1 & \cdots & 0 & 0 \\ \vdots & \vdots & \vdots & \vdots & \vdots \\ 0 & 0 & \cdots & \cos\phi_{n-2} & -1 \\ 0 & 0 & \cdots & 0 & \cos\phi_{n-1} \end{bmatrix} \in \mathbb{R}^{n\times(n-1)}. \tag{38}$$

Vectors $\boldsymbol{p}$, $\boldsymbol{f}$ and $\hat{\boldsymbol{\tau}}$ are defined as $\boldsymbol{p} = [p_1 \ \cdots \ p_n]^T$, $\boldsymbol{f} = [f_1 \ \cdots \ f_{n-1}]^T$ and $\hat{\boldsymbol{\tau}} = [\hat{\tau}_1 \ \cdots \ \hat{\tau}_{n-1}]^T$, respectively. From $\boldsymbol{p}$, we omit the components corresponding to the lifted links and define the resulting vector as $\boldsymbol{r}$. Matrix S is the selection matrix which satisfies $\boldsymbol{p} = S\boldsymbol{r}$. Matrices D and A are defined as $D = D_c|_{\boldsymbol{\phi}=\boldsymbol{0}}$, and $A = -D_c|_{\boldsymbol{\phi}=\boldsymbol{\pi}}$, respectively. Matrices $\bar{S}_\phi$ and $\tilde{S}_\phi$ are defined as follows:

$$\bar{S}_\phi = \begin{bmatrix} \mathrm{diag}(\sin\phi_1, \cdots, \sin\phi_{n-1}) \\ \boldsymbol{0}^T \end{bmatrix} \in \mathbb{R}^{n\times(n-1)}, \tag{39}$$

$$\tilde{S}_\phi = \begin{bmatrix} \boldsymbol{0}^T \\ \mathrm{diag}(\sin\phi_1, \cdots, \sin\phi_{n-1}) \end{bmatrix} \in \mathbb{R}^{n\times(n-1)}. \tag{40}$$

By solving the set of linear equations (34)-(36) for $\boldsymbol{n}$, $\hat{\boldsymbol{\tau}}$, $\boldsymbol{r}$ and $\boldsymbol{f}$, under the condition that $r_i \geq 0$ for all i, i.e., that the normal force from the ground must be non-negative, we can determine necessary joint torques and normal forces from the ground.

Suppose $n_g(\leq n)$ links are grounded, then, there are $3n+n_g-3$ unknowns and $3n$ equations. Therefore, the number of grounded links n_g should intuitively satisfy $n_g \geq 3$ and, in the case of $n_g \geq 4$, we have redundancy in calculating these unknowns. This redundancy can be used to control normal forces, by tuning yaw and pitch torques appropriately; however, in the present paper, we simply use the solution that gives the minimum norm of the pitch torque vector, under the constraint of $r_i \geq 0$ for all i. Note that if $|\phi_i| = \pi/2$, then $\hat{\tau}_i$ does not have any effect on link i, under the assumption that joints have no length. This leads to the possibility that the linear equations (34)-(36) have no solutions. Therefore, we subsequently confine the range of the yaw angles to the range $(-\pi/2, \pi/2)$.

D. Energy Consumption

To calculate the energy consumption of a robot, the energy consumption of a DC motor is evaluated by the following equation [36]:

$$e_{\text{motor}} = \int_0^t \left\{ \max(\tau(\xi)\omega(\xi), 0) + \frac{\gamma}{r_m^2}\tau^2(\xi) \right\} d\xi, \tag{41}$$

where r_m is the gear reduction ratio of the DC motor and γ is the coefficient for the heat energy loss. The first term represents the mechanical power given by the product of the angular velocity ω and the torque τ at the motor. We neglect the effect of negative power because the DC motor does not store the energy supplied by the negative work. The second term represents the heat energy loss.

In [36], this equation was used to calculate the energy consumption of muscle, and in [14] the $\max$ function was omitted for evaluation of the energy consumption of a DC motor. Though these choices make only small differences in the simulation results in V-C, we chose to use (41) because the equation used in [14] clearly underestimates the energy consumption unless some energy storage mechanism is assumed.

Let e_i and $\hat{e}_j$ be the energy consumed at the i-th yaw joint and the j-th pitch joint, respectively. Then, the total energy E_{total} that is consumed by a whole snake robot is

$$E_{\text{total}} = \sum_{i=1}^{n-1} e_i + \sum_{j=1}^{n-1} \hat{e}_j, \tag{42}$$

where e_i and $\hat{e}_j$ are calculated by (41).

IV. Input Torque for Yaw Joints

The equations of motion (32) can be divided into two parts as follows:

$$H_{11}\ddot{\boldsymbol{w}} + H_{12}\ddot{\boldsymbol{\phi}} + \boldsymbol{W}_1 + \boldsymbol{C}_1 = \boldsymbol{0}_{3\times 1} \tag{43}$$

$$H_{21}\ddot{\boldsymbol{w}} + H_{22}\ddot{\boldsymbol{\phi}} + \boldsymbol{W}_2 + \boldsymbol{C}_2 = \boldsymbol{\tau}, \tag{44}$$

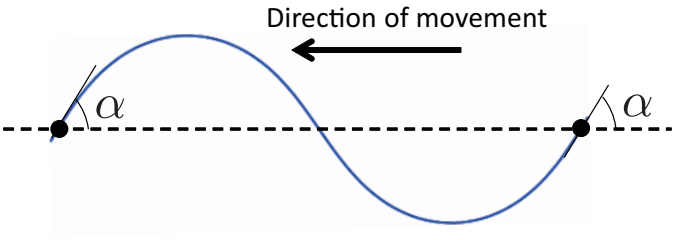

Fig. 8. One period of the serpenoid curve and the definition of winding angle α. Parameter T controls how many serpenoid curves are formed by a snake robot

where $\boldsymbol{w} = [x_h \ y_h \ \theta_1]^T$ and

$$H = \begin{bmatrix} H_{11} & H_{12} \\ H_{21} & H_{22} \end{bmatrix}, \ H_{11} \in \mathbb{R}^{3\times 3}, \ H_{22} \in \mathbb{R}^{(n-1)\times(n-1)}, \tag{45}$$

$$W \mathrm{diag}(J_{q\bar{q}}\dot{\boldsymbol{q}}) J_{q\bar{q}}\dot{\boldsymbol{q}} = \begin{bmatrix} \boldsymbol{W}_1 \\ \boldsymbol{W}_2 \end{bmatrix}, \ \boldsymbol{W}_1 \in \mathbb{R}^3, \ \boldsymbol{W}_2 \in \mathbb{R}^{n-1}, \tag{46}$$

$$C\dot{\boldsymbol{q}} = \begin{bmatrix} \boldsymbol{C}_1 \\ \boldsymbol{C}_2 \end{bmatrix}, \ \boldsymbol{C}_1 \in \mathbb{R}^3, \ \boldsymbol{C}_2 \in \mathbb{R}^{n-1}. \tag{47}$$

Because H_{11} is positive definite, (43) can be solved for $\ddot{\boldsymbol{w}}$ as

$$\ddot{\boldsymbol{w}} = -H_{11}^{-1}(H_{12}\ddot{\boldsymbol{\phi}} + \boldsymbol{W}_1 + \boldsymbol{C}_1). \tag{48}$$

From (44) and (48), it follows that:

$$\begin{aligned} \mathcal{H}\ddot{\boldsymbol{\phi}} + \boldsymbol{W}_2 + \boldsymbol{C}_2 - H_{21}H_{11}^{-1}(\boldsymbol{W}_1 + \boldsymbol{C}_1) &= \boldsymbol{\tau} \\ \mathcal{H} = H_{22} - H_{21}H_{11}^{-1}H_{12}. & \end{aligned} \tag{49}$$

Therefore, by the following controller:

$$\boldsymbol{\tau} = \mathcal{H}\boldsymbol{u} + \boldsymbol{W}_2 + \boldsymbol{C}_2 - H_{21}H_{11}^{-1}(\boldsymbol{W}_1 + \boldsymbol{C}_1), \tag{50}$$

the system can be converted into the following system [9]:

$$\ddot{\boldsymbol{w}} = -H_{11}^{-1}(\boldsymbol{W}_1 + \boldsymbol{C}_1) - H_{11}^{-1}H_{12}\boldsymbol{u} \tag{51}$$

$$\ddot{\boldsymbol{\phi}} = \boldsymbol{u}. \tag{52}$$

We employ the serpenoid curve [10] for the body shape of the robot. The serpenoid curve is defined as a curve whose curvature propagates in sinusoidal manner with respect to the arc-length coordinate. This curve is said to be very similar to the body shape of biological snakes, and is often employed in studies on snake robots [11]–[14], [20].

Let $s \in [0, \ 1]$ be the arc-length coordinate of the points on a curve and $\rho(t, \ s)$ be the curvature at a point s at time t. The serpenoid curve is characterized by

$$\rho(t, \ s) = 2\pi\alpha T \sin(vt - 2\pi T s), \tag{53}$$

where v is the angular frequency of bending, and T indicates how many periods are formed within the interval of $s \in [0, \ 1]$, that is, it represents the spatial frequency of the body shape. The winding angle α indicates the largest angle between the serpenoid curve and the direction of movement, as shown in Fig. 8. The effects of different α and T are illustrated in Fig. 9.

To employ this body shape, yaw joint angles are set according to the following equation:

$$\phi_i = \frac{2\pi T}{n}\alpha \sin\left(vt - \frac{2\pi T}{n}i\right), \quad i = 1, \ \cdots, \ n-1. \tag{54}$$

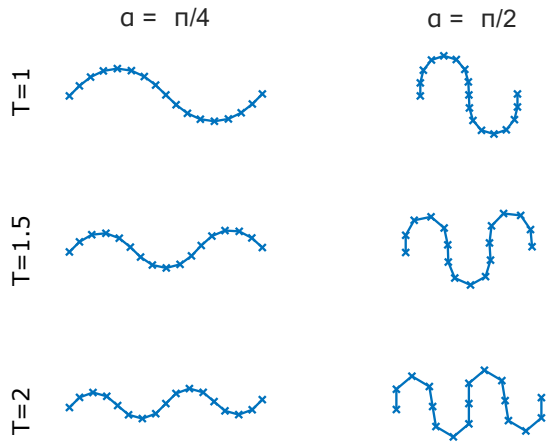

Fig. 9. Robot shapes for different pairs of α and T. A snake robot with 16 links (15 joints) is assumed. Crosses represent the end points of links. T controls how many serpenoid periods are made by the snake robot. The amplitude of the curve is affected both by α and T: a larger T with fixed α leads to a smaller amplitude; a larger α with fixed T leads to a larger amplitude.

Therefore, the angular acceleration of each joint is set as

$$\ddot{\phi}_i = -\frac{2\pi T}{n}\alpha v^2 \sin\left(vt - \frac{2\pi T}{n}i\right). \tag{55}$$

From (50), (52) and (55), the torque input for each yaw joint can be determined to form the serpenoid curve.

V. Simulation

We model the horizontal movement of lifted parts of the robot as frictionless movement in Sec. III-A, that is, we set the viscous coefficients of the lifted links to zero. Further, we assume that the viscous coefficients of link i are proportional to the normal force p_i acting on the link as is assumed in [16]. Therefore, for some constants c_{xo}, c_{yo} and $c_{\theta o}$, the viscous coefficients associated with link i are $c_{x,i} = p_i c_{xo}$, $c_{y,i} = p_i c_{yo}$ and $c_{\theta,i} = p_i c_{\theta o}$. Note that c_{yo} must be larger than c_{xo} to realize lateral undulation [9]. From a consideration of torque acting on a link due to the friction force in the case of pure rotation, $c_{\theta o}$ is set to be $c_{\theta o} = l^2 c_{xo}/3$ [31].

In the remainder of this section, the criteria to simulate sidewinding locomotion and sinus-lifting motion are presented, and the energy efficiency is defined. Section V-D presents simulations of various combinations of friction coefficients. We consider a 16-link snake robot with a total mass of 5.0 kg and a total length of 1.0 m (5/16 kg and 1/16 m for each link) in simulations. Among the three parameters, α, v, and T, that regulate the serpenoid curve, T was fixed at 2, that is, the snake robot makes two periods of waves within its length. For α and v, we simulated various combinations.

A. Criteria for Deciding Lifted and Grounded Parts for Sidewinding Locomotion

In this subsection, we explain how to determine grounded links, and then show that only by choosing lifted and grounded

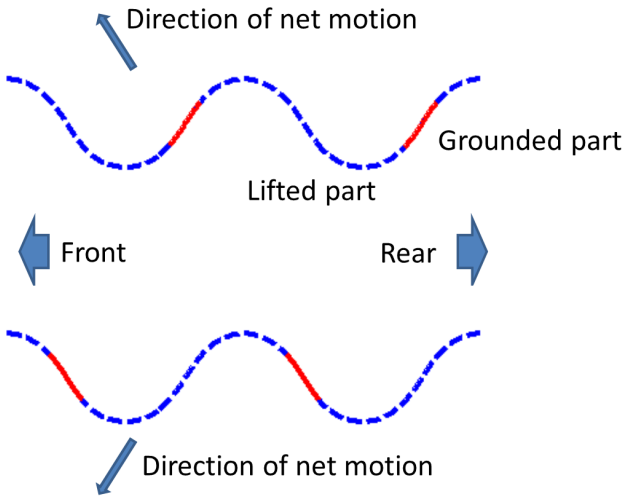

Fig. 10. Relationship between lifting pattern and the direction of net motion, which can be seen from the observation of real snakes. The solid lines correspond to grounded parts and the dashed lines represent lifted parts of the snake robot.

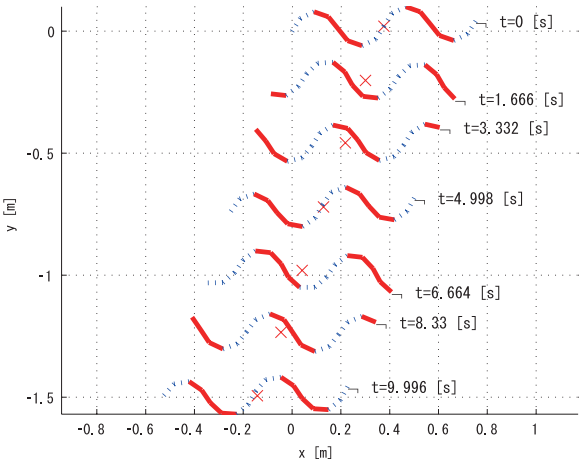

Fig. 11. Simulation result of sidewinding locomotion. Dashed lines represent lifted parts; $\times$ represents the position of the center of mass. The relationship between the grounding pattern and the movement direction is compatible with biological observations.

links appropriately, sidewinding-like locomotion can be generated. Fig. 10 describes the relationship between lifting pattern and direction of net motion, which is derived from observations of biological snakes [6], [37].

In the present study, we decided to use the lifting pattern that is shown in the bottom of Fig. 10. To this end, grounded links are selected as follows: If $|\phi_{i-1}|,\ |\phi_i| < \phi_{\text{th}}$ and $\phi_{i-1} < \phi_i$, then the link i is a grounded link. The threshold of the angle ϕ_{th} is determined using some constant $k_\phi \in (0,\ 1)$ as $\phi_{\text{th}} = k_\phi \phi_{\max}$, where $\phi_{\max} = 2\pi\alpha T/n$ is the amplitude of the joint angles.

For sinus-lifting motion, similar criteria are used, but the direction of the change in curvature is not required to be considered. Therefore, the link i is set to be grounded if $|\phi_{i-1}|,\ |\phi_i| < \phi_{\text{th}}$ is satisfied.

Because the number of grounded links gets smaller with a smaller k_ϕ, it is estimated that with a smaller k_ϕ, we can reduce the energy loss by friction and can improve energy efficiency in some cases. However, this also means that the robot has a smaller supporting polygon, which is the convex-hull of the ground contact points. If the center of mass of the robot is located outside this polygon, equilibrium of the force and torque cannot be attained, and the robot will fall down. Therefore, the required k_ϕ is slightly larger than the minimum that maintains at least four grounded links.

Confirmation of the Criteria: The validity of the criteria for simulating sidewinding locomotion mentioned above is tested by a simulation.

We set the parameters as $T = 2.0$, $\alpha = 1.0$ rad and $v = 5.0$ rad/s. The constants in the viscous coefficients are set to be $c_{xo} = 0.1$ s^2/m and $c_{yo} = 0.5$ s^2/m. The initial configuration is $\boldsymbol{q}(0) = [0\ 0\ \alpha\ \boldsymbol{\phi}(0)^T]^T$, where $\boldsymbol{\phi}(0)$ is determined from (54) by setting $t = 0$. Initial angular velocities for joints are determined according to the time derivative of (54), and $\dot{\boldsymbol{w}}(0)$. The initial velocity of head and angular velocity of link 1 is determined so as to set both the initial velocity of the CM and the initial total angular momentum to zero. Fig. 11 shows the result of simulation, which shows that by this criterion, the same relationship between the grounding pattern and movement direction as biological snakes can be obtained.

B. Criteria for Deciding Lifted and Grounded Parts for Sinus-Lifting Motion

In sinus-lifting motion, a snake lifts up its body parts where the curvature is large; the direction of bending does not matter. To realize this sort of ground contact pattern, a similar decision rule to that for sidewinding locomotion can be used: if $|\phi_{i-1}|, |\phi_i| < \phi_{\text{th}}$, then the link i is a grounded link. Note the difference from the case of sidewinding locomotion. In sidewinding locomotion, the direction of bending should be taken into consideration, but this is unnecessary in sinus-lifting motion.

C. Energy Efficiency

The energy efficiency is defined as the distance that the CM of the robot can travel per unit of energy:

$$(\text{energy efficiency}) = \frac{(\text{distance CM traveled})}{(\text{energy consumption})}. \qquad (56)$$

Greater energy efficiency means that the robot can travel longer distance per unit of energy. Energy consumption of the yaw and pitch joints is calculated according to (41).

The coefficients for heat energy loss and gear reduction ratio for yaw joint motors are $\gamma_{\text{yaw}} = 4.6 \times 10^4\ \Omega(\text{A/Nm})^2$ and $r_{m,\text{yaw}} = 76$, respectively. In contrast, corresponding coefficients for pitch joint motors are $\gamma_{\text{pitch}} = 8.1 \times 10^2\ \Omega(\text{A/Nm})^2$ and $r_{m,\text{pitch}} = 51$, which are the same as given in [14]. In the simulations, k_ϕ was set to be $k_\phi = 1.0$ for sidewinding locomotion, and $k_\phi = 0.92$ for sinus-lifting motion. Note that the number of grounded links is more limited in sidewinding

locomotion than in sinus-lifting motion; thus, a larger k_ϕ is required for sidewinding locomotion than for sinus-lifting motion. Parameter settings for simulations are summarized in Table I. As can be seen in Table I, we continue to use $T = 2$ because if $T < 2$, it is difficult to satisfy the condition of $n_g \geq 3$ in sidewinding locomotion that is generated according to Section V.A.

D. Simulations in Various Environments

We ran simulations for eight different situations, each distinguished by the frictional properties between the robot and the ground: (i) $(c_{xo}, c_{yo}) = (0.01, 0.03)$ s^2/m, (ii) $(c_{xo}, c_{yo}) = (0.1, 0.3)$ s^2/m, (iii) $(c_{xo}, c_{yo}) = (0.01, 0.04)$ s^2/m, (iv) $(c_{xo}, c_{yo}) = (0.1, 0.4)$ s^2/m, (v) $(c_{xo}, c_{yo}) = (0.1, 0.05)$ s^2/m, (vi) $(c_{xo}, c_{yo}) = (0.1, 0.5)$ s^2/m, (vii) $(c_{xo}, c_{yo}) = (0.01, 0.1)$ s^2/m and, (viii) $(c_{xo}, c_{yo}) = (0.1, 1.0)$ s^2/m. The ratios between the two friction coefficients c_{xo}/c_{yo} are 1/3 for (i) and (ii), 1/4 for (iii) and (iv), 1/5 for (v) and (vi) and, 1/10 for (vii) and (viii). This ratio is considered critical for controllability of the lateral undulation [9]. The smaller the ratio is, the more efficient the lateral undulation becomes. We chose 1500 combinations of bending frequency and winding angle (v, α) at random, where $v \in [0.01, 50]$ and $\alpha \in [0.01, 1.4]$.

The results are shown in Fig. 12 as scatter plots. From these plots it can be seen that there is a trade-off between speed and energy efficiency in all three gaits. In Fig. 13, only points that satisfy the trade-off are plotted. Note that most of the trade-off lines do not reach the vertical axis, because no combination of (α, v) was found that attains lower speed with higher energy efficiency than the left most points on those lines. Each of these curves define the maximum energy efficiency as a function of locomotion speed given the gait and the environment. Combinations of α and v which attain these trade-off performances can be seen as solutions to the multiobjective optimization problem which aims to maximize speed and energy efficiency. According to multiobjective optimization, these trade-off curves are called the Pareto fronts, or simply 'fronts'.

1) Comparison between Lateral Undulation and Sidewinding Locomotion: As pointed out in the literature [17], [18], sidewinding locomotion is generally more efficient than lateral undulation. If the overall friction is large, such as in Figs 13(b), 13(d), and 13(f), sidewinding locomotion outperforms lateral undulation at all speeds. However, if the overall friction is small, there are intersections between these fronts. In each of Figs. 13(a), 13(c), 13(e) and 13(g), there is an intersection in low-speed region. For speeds lower than that critical value, lateral undulation is more energy efficient than

TABLE I
PARAMETER SETTINGS FOR SIMULATIONS

m	5/16 kg	n	16
l	1/32 m	γ_{yaw}	4.6 $\times 10^4$ Ω(A/Nm)^2
T	2	γ_{pitch}	8.1 $\times 10^2$ Ω(A/Nm)^2
Simulation time	2.1 periods	$r_{m,\text{yaw}}$	76
k_ϕ for sidewinding	1.0	$r_{m,\text{pitch}}$	51
k_ϕ for sinus-lifting	0.92		

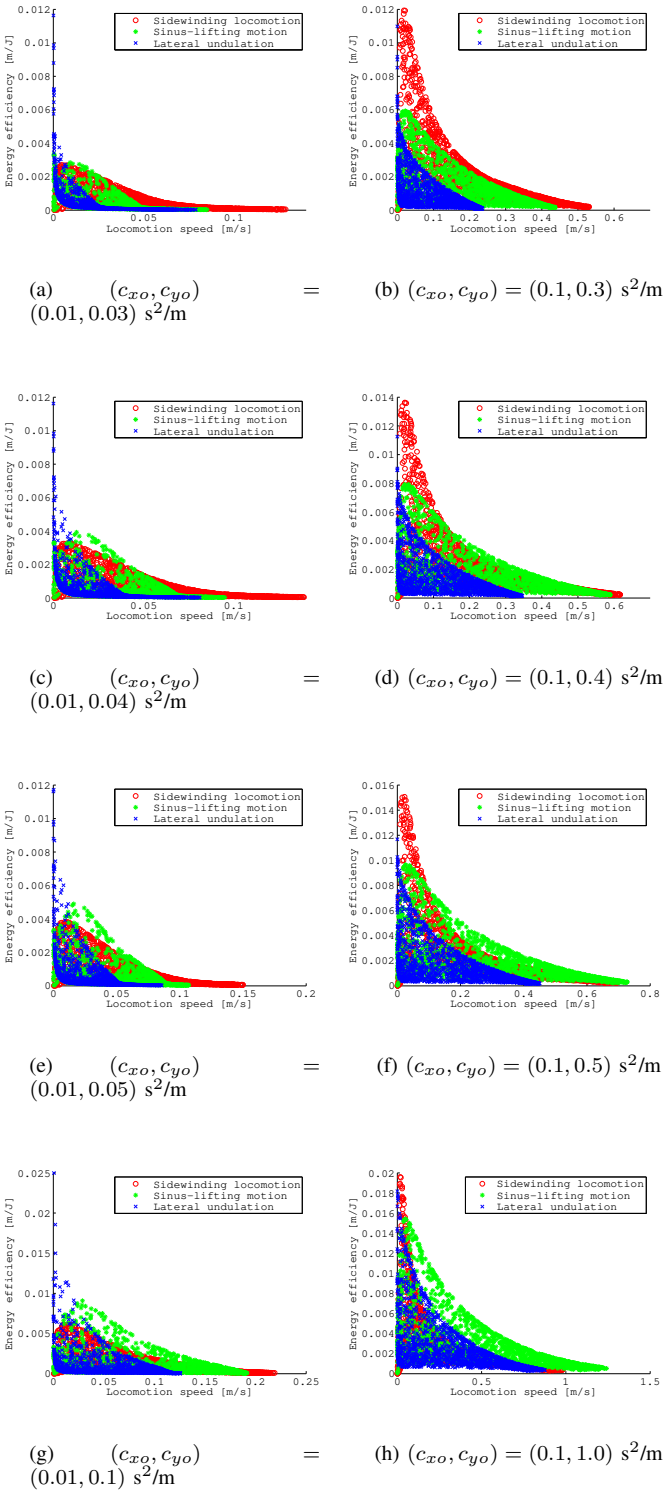

(a) $(c_{xo}, c_{yo}) = (0.01, 0.03)$ s^2/m (b) $(c_{xo}, c_{yo}) = (0.1, 0.3)$ s^2/m

(c) $(c_{xo}, c_{yo}) = (0.01, 0.04)$ s^2/m (d) $(c_{xo}, c_{yo}) = (0.1, 0.4)$ s^2/m

(e) $(c_{xo}, c_{yo}) = (0.01, 0.05)$ s^2/m (f) $(c_{xo}, c_{yo}) = (0.1, 0.5)$ s^2/m

(g) $(c_{xo}, c_{yo}) = (0.01, 0.1)$ s^2/m (h) $(c_{xo}, c_{yo}) = (0.1, 1.0)$ s^2/m

Fig. 12. Scatter plot showing energy efficiency at different locomotion speeds. Blue crosses correspond to the results of lateral undulation, green asterisks to those of sinus-lifting motion and red circles to those of sidewinding locomotion. There is a region of attainable performance in terms of locomotion speed and energy efficiency. Typically maximum efficiency at a certain speed or maximum speed with a certain energy efficiency is desirable. Thus, the set of points representing a trade-off, the Pareto front, is of interest.

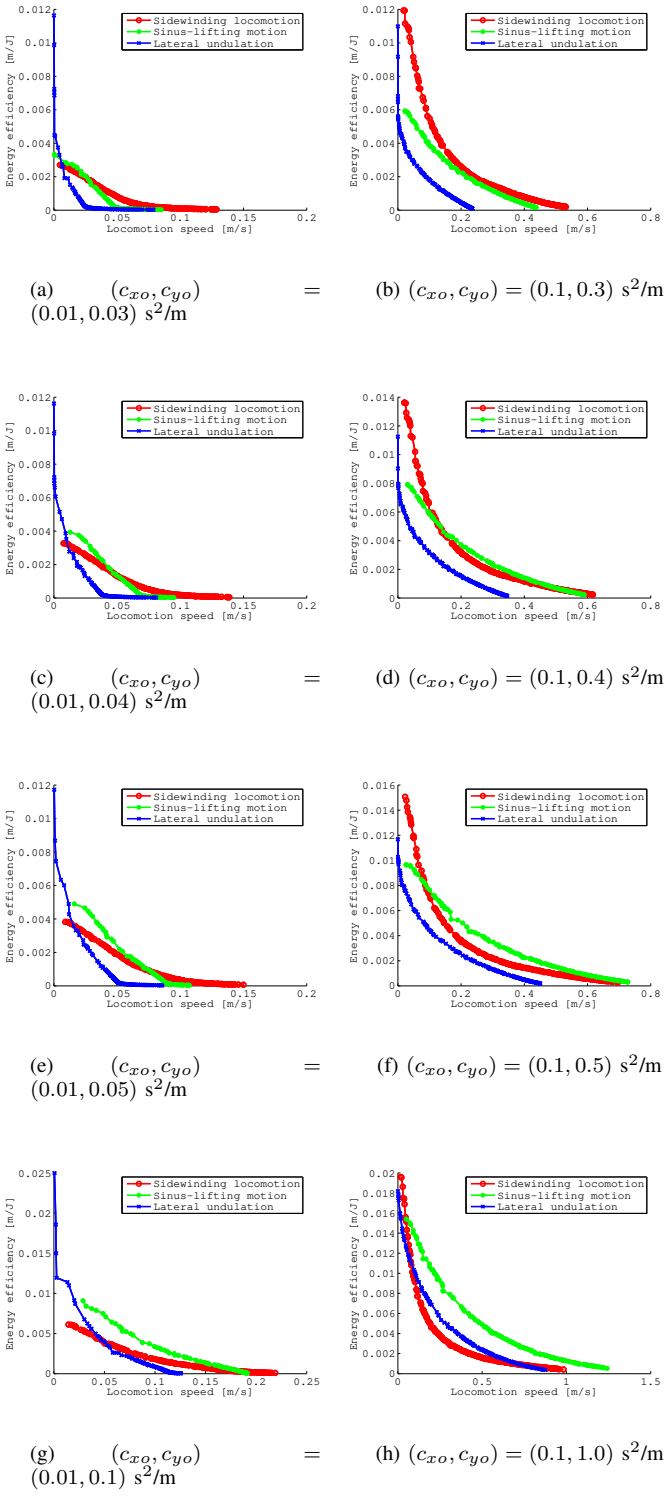

(a) $(c_{xo}, c_{yo}) = (0.01, 0.03)$ s^2/m (b) $(c_{xo}, c_{yo}) = (0.1, 0.3)$ s^2/m

(c) $(c_{xo}, c_{yo}) = (0.01, 0.04)$ s^2/m (d) $(c_{xo}, c_{yo}) = (0.1, 0.4)$ s^2/m

(e) $(c_{xo}, c_{yo}) = (0.01, 0.05)$ s^2/m (f) $(c_{xo}, c_{yo}) = (0.1, 0.5)$ s^2/m

(g) $(c_{xo}, c_{yo}) = (0.01, 0.1)$ s^2/m (h) $(c_{xo}, c_{yo}) = (0.1, 1.0)$ s^2/m

Fig. 13. Pareto fronts discovered through simulations. These fronts define the maximum energy efficiency as a function of locomotion speed or *vice versa*.

sidewinding locomotion. This is consistent with previous literatures [34] stating that sidewinding locomotion is especially good for high speed locomotion. This phenomenon can be understood as follows: When the robot is moving slowly, energy consumed by lifting is dominant, but as speed increases, the dissipation due to friction increases while the energy for lifting remains almost constant. As a consequence, lateral undulation, which loses more energy by dissipation, is less energy efficient than sidewinding locomotion at high speeds. Note that as the ratio c_{xo}/c_{yo} gets smaller, the critical speed gets higher: about 6.5×10^{-3} m/s in Fig. 13(a), 1.1×10^{-2} m/s in Fig. 13(c), 1.5×10^{-2} m/s in Fig. 13(e), and 5.0×10^{-2} m/s in Fig. 13(g). A smaller friction ratio results in higher performance in lateral undulation, but not in sidewinding locomotion. An interesting phenomenon can be seen from Fig. 13(h). There are two intersections between the fronts: one in the low speed region and the other in the high speed region. The energy efficiency of sidewinding locomotion is outperformed by lateral undulation in middle speed region, i.e., sidewinding locomotion is more efficient than the lateral undulation only if the speed is very low or very high. Understanding the cause of this phenomenon is beyond the scope of the present study, and will be the focus of our future work.

2) Comparison between Sidewinding Locomotion and Sinus-lifting Motion: As with sidewinding locomotion, our results show that sinus-lifting motion is generally more efficient than lateral undulation. This is consistent with other works by researchers of snake robots [14]. However, the shapes of the fronts are more similar to those of lateral undulation than sidewinding locomotion. Fronts of sinus-lifting motion and sidewinding locomotion have an intersection or intersections in a wide range of friction setting. If the overall friction is small as in Figs. 13(a), 13(c), 13(e), and 13(g), the fronts of sidewinding locomotion and sinus-lifting motion intersect at a single point. If the speed is lower than that critical value, sinus-lifting motion is more energy efficient than sidewinding locomotion, otherwise sidewinding locomotion is more energy efficient. If the overall friction is relatively large as in Fig. 13(d), these two fronts generally intersect at two points, and sinus-lifting motion is more energy efficient than sidewinding locomotion in the middle speed range. In Figs. 13(f) and 13(h), there is only one intersection, in low-speed region. It is conceivable, however, that, if we were to extend the search space, another intersection would be found in the higher-speed region.

3) Energy Consumed by Pitch Joints: Let the energy consumed by all of the pitch joints be E_{pitch}, and that by the whole robot be E_{total}. Fig. 14 shows the ratio $E_{\text{pitch}}/E_{\text{total}}$ for sidewinding locomotion and sinus-lifting motion (for lateral undulation, the ratio is always 0). Note that the ratio is only calculated for parameter settings that are Pareto optimal. This figure shows that $E_{\text{pitch}}/E_{\text{total}}$ is larger for sidewinding locomotion than that for sinus-lifting motion, because there are more lifted links. Also, in both gaits, the ratio becomes smaller at higher speeds because of the higher dissipation at the grounded links.

4) Effect of the Environment: If the overall friction is low, as in Figs. 13(a), 13(c), 13(e) and 13(g), the gaits are unable to achieve very high locomotion speed. In such environments, slippage hinders the snake robot's movement. In Figs. 15 and 16, movements of sinus-lifting motion and sidewinding locomotion are captured. In both figures, (a) corresponds to the setting $(c_{xo},\ c_{yo}) = (0.01,\ 0.03)$, and (b)

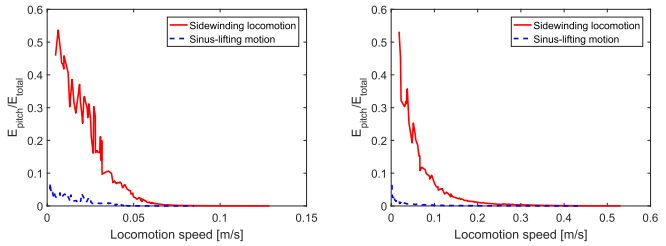

(a) $(c_{xo}, c_{yo}) = (0.01, 0.03)$s^2/m (b) $(c_{xo}, c_{yo}) = (0.1, 0.3)$ s^2/m

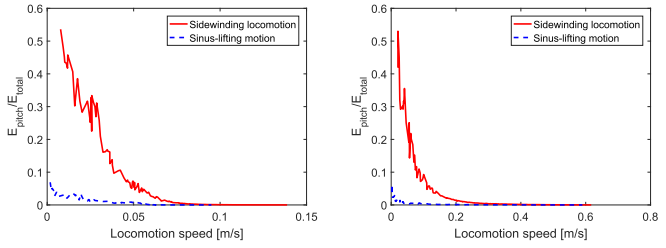

(c) $(c_{xo}, c_{yo}) = (0.01, 0.04)$ s^2/m (d) $(c_{xo}, c_{yo}) = (0.1, 0.4)$ s^2/m

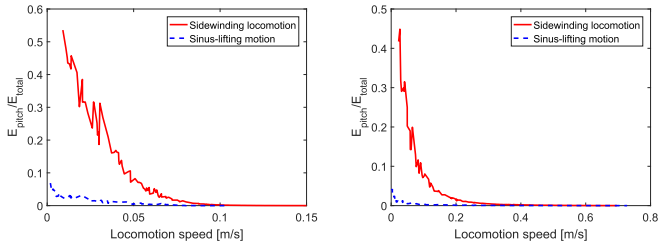

(e) $(c_{xo}, c_{yo}) = (0.01, 0.05)$ s^2/m (f) $(c_{xo}, c_{yo}) = (0.1, 0.5)$ s^2/m

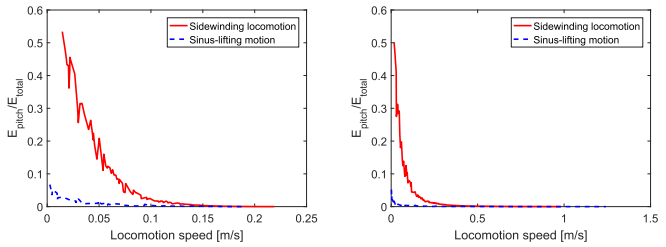

(g) $(c_{xo}, c_{yo}) = (0.01, 0.1)$ s^2/m (h) $(c_{xo}, c_{yo}) = (0.1, 1.0)$ s^2/m

Fig. 14. The ratio between the energy consumed by pitch joints and the total energy $E_{\text{pitch}}/E_{\text{total}}$ for sidewinding locomotion and sinus-lifting motion. The ratio is calculated for those settings on the Pareto fronts. In both gaits, because energy dissipation at the grounded links grows as the locomotion speed increases, the ratio becomes smaller in the higher speed region.

to $(c_{xo},\ c_{yo}) = (0.1,\ 0.3)$. Parameters other than the friction coefficients remain constant, i.e., winding movements of the

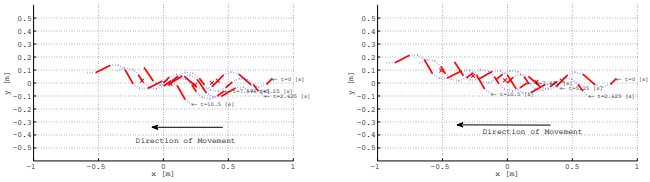

(a) $(c_{xo},\ c_{yo}) = (0.01,\ 0.03)$ (b) $(c_{xo},\ c_{yo}) = (0.1,\ 0.3)$

Fig. 15. Comparison of sinus-lifting motion in different environments. Although the gait is the same, the net displacement is larger for larger friction. This suggests that the slippage prevents the snake robot from moving forward.

snake robot are identical in all plots. Despite this, these figures also show that both gaits result in slower movement in the case of lower friction than in the case of higher friction. This suggests there is greater slippage in low-friction environments that make it difficult for the robot to move fast.

In Fig. 17, the fronts for each gait for various environments are shown. In each figure, c_{xo} is fixed. As c_{yo} becomes larger, i.e. the friction ratio c_{xo}/c_{yo} gets smaller, the efficiency increases in all gaits. However, as can be seen from Fig. 17, the improvement is greater for lateral undulation and sinus-lifting motion than sidewinding locomotion. Large c_{yo} leads to less side-slip and a larger resistance force in the lateral direction, leading to better energy efficiency in lateral undulation and sinus-lifting motion. Fig. 15 shows that a larger resistance force in the lateral direction provides a larger propulsive force for sinus-lifting motion, as the direction of movement is more or less perpendicular to the grounded links. The cause of the improvement in lateral undulation is essentially the same as in sinus-lifting motion. In contrast, in sidewinding locomotion the increase in lateral resistance has a smaller effect on propulsive force, as the direction of movement is more parallel than perpendicular to the grounded links, as shown in Fig. 16. From Fig. 17, the effect of doubling c_{yo} for sidewinding locomotion, which can be seen from the difference by changing c_{yo} from 0.5 s^2/m to 1.0 s^2/m or from 0.05 s^2/m to 0.1 s^2/m, would be 1/4 to 1/2 that for sinus-lifting motion. These results confirm that, for sidewinding locomotion, the anisotropy in friction is not essential. This can be interpreted as a major reason for desert snakes preferring this locomotion. Because snakes' bodies can be easily buried in sandy environments, it is difficult to achieve the required anisotropy.

5) Summary: Both sidewinding locomotion and sinus-lifting motion are generally more energy efficient than lateral undulation, as shown by Fig. 13. However, details change according to the properties of friction. If the anisotropy in friction is large enough, as in Figs. 13(g) and 13(h), sinus-lifting motion is the most efficient of the three gaits; otherwise, sidewinding locomotion is. In the case where the overall friction is small, as in Figs. 13(a), 13(c), 13(e), and 13(g), the most energy efficient performance of these three gaits changes from lateral undulation, then to sinus-lifting motion, and finally

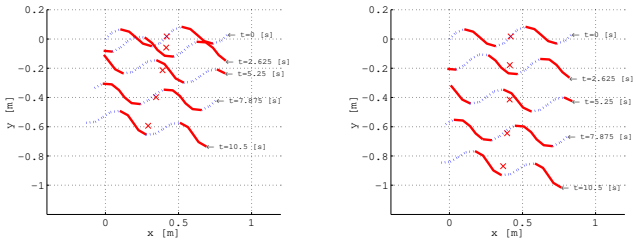

(a) $(c_{xo},\ c_{yo}) = (0.01,\ 0.03)$ (b) $(c_{xo},\ c_{yo}) = (0.1,\ 0.3)$

Fig. 16. Comparison of sidewinding locomotion in different environments. As for sinus-lifting motion, slippage prevents the snake robot from moving in the low-friction environment.

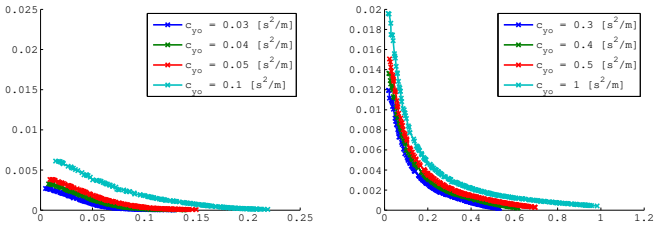

(a) Sidewinding locomotion ($c_{xo} = 0.01$) (b) Sidewinding locomotion ($c_{xo} = 0.1$)

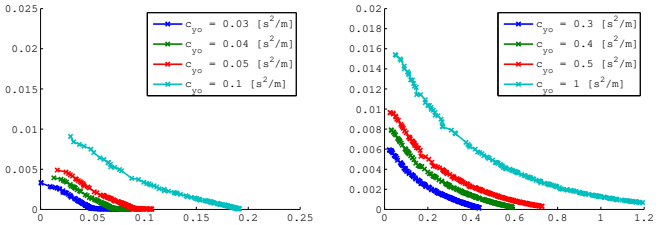

(c) Sinus-lifting motion ($c_{xo} = 0.01$) (d) Sinus-lifting motion ($c_{xo} = 0.1$)

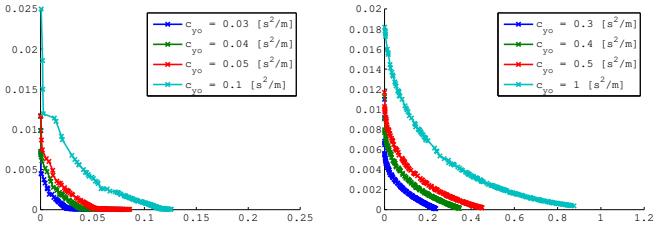

(e) Lateral undulation ($c_{xo} = 0.01$) (f) Lateral undulation ($c_{xo} = 0.1$)

Fig. 17. Plots of Pareto fronts for each locomotion in various environments. In all three gaits, the energy efficiency improves as c_{yo} gets larger. However, the improvement is smaller in sidewinding locomotion than in the other two gaits.

sidewinding locomotion, as the locomotion speed grows. In the case where overall friction is large and friction ratio c_{xo}/c_{yo} is also large, as in Fig 13(b), sidewinding locomotion is the most energy efficient gait. As the friction ratio gets smaller, i.e., as the anisotropy gets more intense, the relative superiority of sidewinding locomotion over the other gaits shrinks, as in Figs. 13(d), 13(f), and 13(h). From [7], the friction ratio for biological snakes was shown to be between 1/3 and 1/2, at least on the flat dry metal surface on which experiments were conducted, which seems to be rather small. Previous studies have suggested that biological snakes may also use obstacles such as rocks to gain a propulsive force by pushing against them [7], [10]. Therefore, we speculate that some snakes use sidewinding locomotion on flat surfaces because they cannot gain enough propulsive force to overcome the resistive force; thus, sidewinding locomotion outperforms other gaits in such situations. Where anisotropy in friction is large enough or where there are enough obstacles to compensate for the lack of anisotropy in friction, sinus-lifting motion becomes the most efficient gait, especially at higher speeds. This seems to be consistent with biological snakes that often use sinus-lifting motion when moving at high speed. However, snake robots typically employ passive wheels, leading to intense anisotropy. Therefore, if the environment is flat and solid enough to support it, sinus-lifting motion will be the most energy efficient gait.

VI. Conclusion

In the present paper, a dynamic analysis of sidewinding locomotion, sinus-lifting motion and lateral undulation by a snake-like robot was presented. Sidewinding locomotion and sinus-lifting motion were treated as planar locomotion for simplicity, and the normal forces acting on the grounded links and the torques applied on pitch joints were calculated by solving equilibrium equations. Assuming viscous friction between the robot and the environment, sidewinding locomotion and sinus-lifting motion were simulated by selecting grounded links so as to make the grounded pattern similar to that of biological snakes. Simulation results show there are speed–energy efficiency trade-offs in both sidewinding locomotion and sinus-lifting motion gaits. Investigation of the curves of these trade-off points, or Pareto fronts, verified hypotheses that sidewinding locomotion is efficient especially when moving at high speed. These fronts also clarified that if the anisotropy in friction is great enough, and overall friction is large, even lateral undulation outperforms sidewinding locomotion in wide range of locomotion speeds. In the same way, sinus-lifting motion is shown to be efficient generally, but its front has intersections with fronts of other gaits, resulting in the most energy efficient gait changing as the locomotion speed changes.

In the present study, links to be grounded and lifted were predefined based on the curvature of the body shape. However, to maximize the effect of lifting, the grounded and lifted links should be determined according to the situation. This will require a combinatorial optimization method. Another possible topic for future research is analysis using a three-dimensional dynamic model. In the present study, movements

in the vertical direction are assumed to be small enough to be neglected, but this assumption will be true only in the case of small amplitudes of angular acceleration in pitch joints. These improvements will require a large calculation cost, prohibiting random searches such as in the present study. However, since it has been shown that there is a trade-off between locomotion speed and energy efficiency, and since we generally are not interested in performances which is not on the front, we can use some multiobjective optimization algorithm for expensive black-box functions, such as proposed in [38]–[39].

REFERENCES

[1] M. Travers, C. Gong, and H. Choset, "Shape-Constrained Whole-Body Adaptivity," in *Proc. IEEE International Symposium on Safety, Security, and Rescue Robotics*, pp.1-6, 2015.

[2] P. Liljebäck, K.Y. Pettersen, Ø. Stavdahl, and J.T. Gravdahl, "Hybrid Modeling and Control of Obstacle-Aided Snake Robot Locomotion," *IEEE Trans. Robot.*, vol. 26, no. 5, pp. 781-799, 2010.

[3] C. Gong, D.I. Goldman, and H. Choset, "Simplifying Gait Design via Shape Basis Optimization," Robotics: Science and Systems Conference, 2016.

[4] E. Kelasidi, P. Liljebäck, K.Y. Pettersen, and J.T. Gravdahl, "Experimental Investigation of Efficient Locomotion of Underwater Snake Robots for Lateral Undulation and Eel-like Motion Patterns," *Robotics and biomimetics*, vol. 2, no. 8, 2015.

[5] S.A. Stamper, S. Sefati, and N.J. Cowan, "Snake Robot Uncovers Secrets to Sidewinders' Maneuverability," *Proceedings of the National Academy of Sciences*, vol. 112, no. 19, pp. 5870-5871, 2015.

[6] J. Gray, "The Mechanism of Locomotion in Snakes," *J. Exp. Biol.*, vol. 23, no. 2, pp. 101-123, 1946

[7] J. Gray, and H. W. Lissmann, "The Kinetics of Locomotion of the Grass-Snake," *J. Exp. Biol.*, vol. 26, no. 4, pp. 354-367, 1950

[8] J.E. Baio, M. Spinner, C. Jaye, D.A. Fischer, S.N. Gorb, and T. Weidner, "Evidence of a molecular boundary lubricant at snakeskin surfaces," *J. R. Soc. Interface*, vol 12, no. 113, 2015

[9] P. Liljebäck, K. Pettersen, Ø. Stavdahl, and J. Gravdahl, "Controllability and Stability Analysis of Planar Snake Robot Locomotion," *IEEE Trans. Autom. Control*, vol. 56, no. 6, pp. 1365-1380, 2011

[10] S. Hirose, *Biologically Inspired Robots: Snake-Like Locomotors and Manipulators*. Oxford University Press, 1993

[11] M. Tanaka, and F. Matsuno, "A Study on Sinus-lifting Motion of a Snake Robot with Switching Constraints," in *Proc. IEEE Int. Conf. Robot. Autom.*, 2009, pp. 2270-2275

[12] K. Shigeta, H. Date, S. Nakaura, and M. Sampei, "Improvement of Manipulability for Locomotion of a Snake Robot by Mass Distribution," in *Proc. of the 41st SICE Annual Conference*, Vol. 4, pp. 2214-2217, 2002

[13] S. Ma, Y. Ohmameuda, and K. Inoue, "Dynamic Analysis of 3-dimensional Snake Robots," in *Proc. IEEE/RSJ Int. Conf. Intell. Robots Syst.*, 2004, pp.767-772

[14] S. Toyoshima, M. Tanaka, and F. Matsuno, "A Study on Sinus-Lifting Motion of a Snake Robot with Sequential Optimization of a Hybrid System," *IEEE Trans. Autom. Science and Engineering*, vol. 11, no. 1, pp. 139-144, 2014

[15] P. Liljebäck, K. Pettersen, and Ø. Stavdahl, "Modelling and control of obstacle-aided snake robot locomotion based on jam resolution," in *Proc. IEEE Int. Conf. Robot. Autom.*, 2009, pp. 3807-3814

[16] G. Hicks, and K. Ito, "A Method for Determination of Optimal Gaits With Application to a Snake-Like Serial-Link Structure," *IEEE Trans. Autom. Control,*, vol. 50, no. 9, pp. 1291-1306, 2005

[17] J. W. Burdick, J. Radford, and G. S. Chirikjian, "A "Sidewinding" Locomotion Gait for Hyper-Redundant Robots," in *Proc. IEEE Int. Conf. Robot. Autom.*, 1993, pp. 101-106

[18] S. Kelly and R. Murray, "Geometric Phases and Robotic Locomotion," *J. Robotic Systems*, vol. 12, no. 6, pp. 417-431, 1995

[19] I. Tanev, T. Ray, and A. Buller, "Automated Evolutionary Design, Robustness, and Adaptation of Sidewinding Locomotion of a Simulated Snake-Like Robot," *IEEE Trans. Robot.*, vol. 21, no. 4, pp. 632-645, 2005

[20] A. A. Transeth, R. I. Leine, and K. Y. Pettersen, "3-D Snake Robot Motion: Nonsmooth Modeling, Simulations, and Experiments," *IEEE Trans. Robot.*, vol. 24, no. 2, pp. 361-376, 2008

[21] H. Yamada and S. Hirose, "Study of a 2-DOF Joint for the Small Active Cord Mechanism," in *Proc. IEEE Int. Conf. Robot. Autom.*, 2009, pp. 3827-3832

[22] R. Hatton and H. Choset, "Sidewinding on Slopes," in *Proc. IEEE Int. Conf. Robot. Autom.*, 2010, pp. 691-696

[23] K. Melo, "Modular Snake Robot Velocity for Side-Winding Gaits," in *Proc. IEEE Int. Conf. Robot. Autom.*, pp. 3716-3722, 2015

[24] H.C. Astley, C. Gong, J. Dai, M. Travers, M.M. Serrano, P.A. Vela, H. Choset, J.R. Mendelson III, D.L. Hu, and D.I. Goldman, "Modulation of Orthogonal Body Waves Enables High Maneuverability in Sidewinding Locomotion," *Proceedings of the National Academy of Sciences*, vol. 112, no. 19, pp. 6200-6205, 2015.

[25] M. Tesch, K. Lipkin, I. Brown, R. Hatton, A. Peck, J. Rembisz, and H. Choset, "Parametrized and Scripted Gaits for Modular Snake Robots," *Adv. Robotics*, vol. 23, no. 9, pp. 1131-1158, 2009

[26] H. Marvi, C. Gong, N. Gravish, H. Astley, M. Travers, R.L. Hatton, J.R. Mendelson III, H. Choset, D.L. Hu, and D. Goldman, "Sidewinding with Minimal Slip: Snake and Robot Ascent of Sandy Slopes," *Science*, vol. 346, no. 6206, pp. 224-229, 2014

[27] P. Liljebäck, I.U. Haugstuen, and K.Y. Pettersen, "Path Following Control of Planar Snake Robots Using a Cascaded Approach," *IEEE Trans. Control Syst. Tech.*, vol. 20, no. 1, pp. 111–126, 2012

[28] P. Liljebäck, K.Y. Pettersen, Ø. Stavdahl, and J.T. Gravdahl, "Lateral undulation of snake robots: a simplified model and fundamental properties," *Robotica*, Available on CJO 2013 doi:10.1017/S0263574713000295

[29] E. Rezapour, K.Y. Pettersen, P. Liljebäck, and J.T. Gravdahl, "Differential Geometric Modelling and Robust Path Following Control of Snake Robots Using Sliding Mode Techniques," in *Proc. IEEE Int. Conf. Robot. Autom.*, 2014, pp. 4532-4539.

[30] X. Guo, S. Ma, B. Li, M. Wang, and Y. Wang, "Modeling and Optimal Torque Control of a Snake-like Robot Based on the Fiber Bundle Theory," Science China Information Sciences, vol 58, no. 3, pp. 1-13, 2015

[31] M. Saito, M. Fukaya, and T. Iwasaki, "Serpentine Locomotion with Robotic Snakes," *IEEE Control Syst. Mag.*, vol. 22, no. 1, pp. 64-81, 2002

[32] R. Ariizumi, and F. Matsuno, "Dynamical Analysis of Sidewinding Locomotion by a Snake-Like Robot," in *Proc. IEEE Int. Conf. Robot. Autom.*, 2013, pp. 5149-5154

[33] [Online]. Available: http://www.youtube.com/watch?v=zEto1-ZTbd4&list=PL2F7D624D8E886E68&index=11

[34] W. Mosauer, "The Reptiles of a Sand Dune Area and Its Surroundings in the Colorado Desert, California: A Study in Habitat Preference," *Ecology*, vol. 16, no. 1, pp. 13-27, 1935

[35] G. Vossoughi, H. Pendar, Z. Heidari, and S. Mohammadi, "Assisted passive snake-like robots: conception and dynamic modeling using Gibbs-Appell method," *Robotica*, vol. 26, no. 3, pp. 267–276, 2008

[36] J. Nishii, "Legged insects select the optimal locomotor pattern based on the energetic cost," *Biological Cybernetics*, vol. 83, no. 5, pp. 435-442, 2000

[37] W. Mosauer, "On the Locomotion of Snakes," *Science*, vol. 76, no. 1982, pp. 583–585, 1932

[38] M. Tesch, J. Schneider, and H. Choset, "Expensive Multiobjective Optimization for Robotics," in *IEEE Int. Conf. Robot. Autom.*, 2013. 973-980

[39] R. Ariizumi, M. Tesch, K. Kato, H. Choset, and F. Matsuno, "Multiobjective Optimization Based on Expensive Robotic Experiments under Heteroscedastic Noise," *IEEE Trans. Robot.*, doi: 10.1109/TRO.2016.2632739.

PLACE PHOTO HERE

Ryo Ariizumi received BS, ME, and PhD degrees in engineering from Kyoto University in 2010, 2012, and 2015, respectively. He was also a postdoctoral researcher at Kyoto University, and is currently an assistant professor at Nagoya University. His current research interests include control of redundant robots, and optimization of robotic systems.

PLACE
PHOTO
HERE

Fumitoshi Matsuno (M'94) received a Dr Eng from Osaka University, Osaka, Japan, in 1986. In 1986, he joined the Department of Control Engineering, Osaka University. He became a lecturer in the Department of Systems Engineering, Kobe University, in 1991 and an associate professor in 1992. In 1996, he joined the Department of Computational Intelligence and Systems Science, Interdisciplinary Graduate School of Science and Engineering, Tokyo Institute of Technology, as an associate professor. In 2003, he became a professor with the Department of Mechanical Engineering and Intelligent Systems, University of Electro-Communications. Since 2009, he has been a professor with the Department of Mechanical Engineering and Science, Kyoto University, Kyoto, Japan. He is also the Vice-President of NPO International Rescue Systems Institute (IRS). His current research interests include robotics, control of distributed parameter systems and nonlinear systems, rescue support systems in fires and disasters, and swarm intelligence.

Dr. Matsuno has received many awards, including Outstanding Paper Awards in 2001 and 2006, the Takeda Memorial Prize in 2001 from the Society of Instrument and Control Engineers (SICE), and the Outstanding Paper Award in 2013 from the Information Processing Society of Japan. He is a fellow member of SICE and of the Japan Society of Mechanical Engineers, and he is a member of IEEE, the Robotics Society of Japan, and the Institute of Systems, Control and Information Engineers, among other organizations. He served as the co-chair of the IEEE Robotics and Automation Society Technical Committee on Safety, Security, and Rescue Robotics, and the chair of the Steering Committee of the SICE Annual Conference. He is currently an editor for the *Journal of Intelligent and Robotic Systems*, an associate editor for *Advanced Robotics* and *International Journal of Control, Automation, and Systems* among others, and an editorial board member with the Conference Editorial Board of the IEEE Control Systems Society.